Photoproduction of Charged Mesons from Free Nucleons for Bombarding Gamma-Ray Energies Near 275 MeV*

D. GARELICK† AND G. COOPERSTEIN

Laboratory for Nuclear Science and Physics Department, Massachusetts Institute of Technology, Cambridge, Massachusetts

(Received 13 April 1964; revised manuscript received 10 June 1964)

The differential cross section for the photoproduction of a π^- meson from the neutron bound in the deuteron was measured for pion laboratory angles of 76°, 96°, and 118° at incident gamma-ray energies in the region of 275 MeV. The π^- meson and the high-energy proton were detected. The pion momentum and angle were measured by sets of spark chambers situated in front of and behind a magnetic field. The proton angle and range were also measured with spark chambers. To calculate "free" neutron cross sections from our data, we used a modified version of the extrapolation method suggested by Chew and Low. By observing the π^+ only, the differential cross section for π^+ photoproduction from hydrogen also was measured. As determined by this experiment, the differential cross section for photoproduction of a π^- meson from a "free" neutron and the differential cross section for photoproduction of a π^+ meson from hydrogen are as follows:

$E_{\gamma\text{lab}} \simeq 275$ MeV

Reaction	Pion center-of-mass angle	Differential cross section in center-of-mass system (μb/sr)
$\gamma+n\rightarrow\pi^-+p$	92°	17.5±2.6
$\gamma+n\rightarrow\pi^-+p$	112°	18.7±2.8
$\gamma+n\rightarrow\pi^-+p$	132°	17.2±2.6
$\gamma+p\rightarrow\pi^++n$	92°	18.7±2.0
$\gamma+p\rightarrow\pi^++n$	112°	17.7±1.9
$\gamma+p\rightarrow\pi^++n$	132°	16.7±1.8

These results disagree with the dispersion theory predictions of Chew, Goldberger, Low, and Nambu. They also disagree with McKinley's dispersion theory calculations which include a bipion or ρ-meson term in the production amplitudes.

I. INTRODUCTION

BECAUSE there are no high-density free-neutron targets, the cross section for the photoproduction of π mesons from unbound neutrons can only be measured indirectly. Most previous determinations of this cross section for bombarding gamma-ray energies above 200 MeV are inferred from measurements of the relative yields of single π^- and π^+ mesons from deuterium bombarded by electron bremsstrahlung.[1–9] In these experiments, the pion laboratory angle and its momentum are fixed. However, because there are three particles in the final state, this kinematic constraint is not sufficient to ascertain the energy of the bombarding gamma ray or the energies and angles of the other particles involved in the production process.

The relationship between the measured pion yields from deuterium and the free nucleon cross sections is simplified by the following two facts: In the deuteron, the proton and the neutron experience the same potential; and in π^- and π^+ production, the final states are charge symmetric. Nevertheless, in relating these deuterium measurements to the free cross section, several complications arise.

First, the small Coulomb interactions present in the π^- two proton final state are absent in the π^+ two-neutron final state.[10]

Second, in production from deuterium, the final states contain two identical nucleons, and therefore the Pauli principle must be taken into account. This limitation of the final states available to the production and the final-state Coulomb interactions may have different fractional effects on the π^- and on the π^+ yields.

Third, the cross section for the photoproduction of π mesons from free nucleons changes rapidly in the region of the first resonance. Because the production from deuterium involves three particles, the correspondence between the deuterium cross sections for production π^- and π^+ mesons at a given angle and momentum and the free nucleon cross sections as a function of the center-of-mass angle and energy depends upon our knowledge of the momentum distribution of the target nucleon. In particular, the cross sections for meson production

* This work is supported in part through funds provided by the U. S. Atomic Energy Commission under Contract AT(30-1)-2098.

† This paper is based on a thesis submitted in partial fulfillment of the requirements for the degree of Doctor of Philosophy at the Massachusetts Institute of Technology, Cambridge, Massachusetts; October 1963.

[1] I. L. Lebow, B. T. Feld, D. H. Frisch, and L. S. Osborne, Phys. Rev. **85**, 681 (1952).

[2] R. S. White, M. J. Jacobson, and A. G. Schultz, Phys. Rev. **88**, 836 (1952).

[3] R. M. Littauer, D. Walker, Phys. Rev. **86**, 838 (1952).

[4] T. L. Jenkins, D. Luckey, T. R. Palfrey, and R. R. Wilson, Phys. Rev. **95**, 179 (1954).

[5] M. Sands, J. G. Teasdale, and R. L. Walker, Phys. Rev. **95**, 592 (1954).

[6] M. Beneventano, G. Bernardini, G. Stoppini, and L. Tau, Nuovo Cimento **10**, 1109 (1958).

[7] R. H. Land, Phys. Rev. **113**, 1141 (1959).

[8] G. Neugebauer, W. Wales, and R. L. Walker, Phys. Rev. **119**, 1726 (1960).

[9] W. R. Hogg, Proc. Phys. Soc. (London) **80**, 729 (1962).

[10] A. Baldin, Nuovo Cimento **8**, 569 (1958).

from deuterium are influenced by the high-momentum components of the deuteron wave function, and in this region the wave function is not known exactly.

To determine the importance of nucleon binding effects in pion production from deuterium, Land performed a measurement of the relative yields of π^- and π^+ mesons from deuterium bombarded by 290-MeV "monochromatic" gamma rays.[7] His results for backward pion production angles showed that the negative-to-positive ratio measured with a bremsstrahlung beam differed from the ratio measured with monochromatic gamma rays.

To circumvent some of the problems of using the neutron in the deuteron as a neutron target, Chew and Low suggested that cross sections be measured with the kinematics of collisions completely determined.[11] Such measurements might then be categorized according to the momentum transferred to the spectator particle. They further pointed out that the distribution in spectator momentum of the observed events could be predicted if it were assumed that the spectator particle did not take part in the production process. A comparison of the predicted and measured spectra would then test the validity of the assumption. In addition, the data could be extrapolated to negative spectator energies where effects of neutron binding are known exactly, and the effects of final-state interactions vanish. This approach of Chew and Low greatly influenced the design of our experiment and the analysis of our data.

For our experiment, we measured the cross section for the photoproduction of π^- mesons from deuterium using bombarding gamma-ray energies in the region of 275 MeV. Our decision to do this experiment was based upon the observation that the negative-to-positive ratios measured with "monochromatic" gamma rays and the negative-to-positive ratios measured with bremsstrahlung do not agree with the ratios for free nucleons predicted according to dispersion theory by Chew, Goldberger, Low, and Nambu.[12]

II. THEORY RELATING DEUTERIUM CROSS SECTION TO FREE NUCLEON CROSS SECTION

The relationship between the cross section for the photoproduction of a π^- meson from a free neutron and from deuterium is derived in the following manner. We write the cross section for the two-body reaction

$$\gamma+n\rightarrow\pi^-+p \tag{1}$$

in terms of laboratory variables as[13]

$$\frac{d\sigma}{d\Omega_\pi}=\frac{1}{(8\pi)^2}\frac{P_\pi{}^3}{E_\gamma m_n}\frac{|M_2(w,\theta_{\text{c.m.}})|^2}{[(E_\gamma+m_n)P_\pi{}^2-E_\pi(\mathbf{P}_\gamma\cdot\mathbf{P}_\pi)]}, \tag{2}$$

where m_x, E_x, and $\mathbf{P}_x$ denote the mass, total energy, and vector momentum, respectively, of a particle x in reaction (1); $M_2(w,\theta_{\text{c.m.}})$ denotes the matrix element for that reaction; w denotes the total energy in the π^-p center-of-mass system, and $\theta_{\text{c.m.}}$ is the angle of the π^- relative to the incident gamma-ray direction in this system. The units are $\hbar=c=1$.

In contrast, we cannot state the cross section for the photoproduction of π^- mesons from deuterium unless we make some simplifying assumptions because we are ignorant of the role played by the proton in the deuteron during the production process.

If we assume that the spectator particle neither takes part in the production process nor interacts with the other outgoing particles, then its momentum before and after the collision will be the same. Also, the momentum wave function of the spectator proton will be the same before and after the collision because the interaction Hamiltonian governing the production will be the same as in free production, reaction (1). Therefore, the matrix element for production will be a product of the deuteron momentum wave function φ_{P_s} and the matrix element for reaction (1), $M_2(w,\theta_{\text{c.m.}})$. Thus, we can write the cross section for the reaction

$$\gamma+D\rightarrow p+p_s+\pi^- \tag{3}$$

in terms of laboratory variables as[13]:

$$\frac{d^3\sigma}{d\Omega_p d\Omega_\pi dP_\pi}=\frac{|M_2|^2|\varphi_{P_s}|^2}{(4\pi)^5}\frac{P_p{}^3P_\pi{}^2}{E_\gamma m_D E_\pi}\times\frac{1}{[P_p{}^2(E_\gamma+m_D-E_\pi)-E_p\mathbf{P}_p\cdot(\mathbf{P}_\gamma-\mathbf{P}_\pi)]}, \tag{4}$$

where the subscript s denotes the spectator proton, and the kinematic variables are defined in the same way as those in expression (2).

However, this expression contains the deuteron wave function φ_{P_s} which is not known exactly. The true deuteron wave function φ_{P_s} can be separated into an asymptotic part $\varphi_{P_s}{}^A$ and a part resulting from the potential $\varphi_{P_s}{}^V$. The asymptotic wave function is the solution to the deuteron wave equation for neutron-proton separations beyond the range of the neutron-proton potential, and therefore it depends only on the value of the deuteron binding energy. The quantity $\varphi_{P_s}{}^V$ is the solution to the wave equation for neutron-proton separations within the range of the potential and depends on the details of the potential. Thus, we can write

$$\varphi_{P_s}=\varphi_{P_s}{}^A+\varphi_{P_s}{}^V.$$

Using the effective range theory of low-energy neutron-proton interactions, we may evaluate $\varphi_{P_s}{}^A$ as[14,15]

$$\varphi_{P_s}{}^A=\left[\frac{16\pi m_D m_p\alpha}{(1-\alpha r_0)m_n}\right]^{1/2}\frac{1}{(P_s{}^2+\alpha^2)}. \tag{5}$$

[11] G. F. Chew and F. E. Low, Phys. Rev. **113**, 1640 (1959).
[12] G. F. Chew, M. L. Goldberger, F. E. Low, and Y. Nambu, Phys. Rev. **106**, 1345 (1957).
[13] R. P. Feyman, *Theory of Fundamental Processes* (W. A. Benjamin, Inc., New York, 1962).
[14] F. E. Low, *Brandeis University 1959 Summer Institute in Theoretical Physics, Lecture Notes* (Brandeis University, Waltham, Massachusetts, 1959).
[15] Blatt and Weisskopf, *Theoretical Nuclear Physics* (John Wiley & Sons, Inc., New York, 1952).

Here, α is determined by the deuteron binding energy and is equal to 45.8 MeV/c; $r_0=0.882\times10^{-2}$ (MeV/c)$^{-1}$ is the triplet effective range,[16] and $1/(1-\alpha r_0)$ is equal to

$$\left(\int_0^\infty |\varphi_{R_s}{}^A|^2 d^3\mathbf{R}_s\right)\Big/\left(\int_0^\infty |\varphi_{R_s}|^2 d^3\mathbf{R}_s\right)$$

when the asymptotic wave function is normalized in order to equal the true deuteron wave function for internucleon separations R_s greater than the range of the proton-neutron potential. The asymptotic wave function $\varphi_{P_s}{}^A$ is normalized so that if φ_{P_s}, the deuteron wave function, is replaced by $\varphi_{P_s}{}^A$, then

$$\int \frac{d^3\sigma}{d\Omega_\pi dP_s d\Omega_s} P_s{}^2 dP_s d\Omega_s$$

approaches $1/(1-\alpha r_0)$ times the two-body cross section for reaction (1), $d\sigma/d\Omega_\pi|_{\text{free}}$, in the limit of α^2, or the deuteron binding energy, approaching zero.

Furthermore, it is significant that $\varphi_{P_s}{}^A$ has a pole at $P_s{}^2=-\alpha^2$. For any reasonably behaved neutron-proton potential, the true deuteron wave function φ_{P_s} does not have any additional poles in the region about $P_s{}^2=-\alpha^2$.[11,14] In other words, the true deuteron wave function approaches the asymptotic wave function in the limit as $P_s{}^2$ approaches $-\alpha^2$. In general, then, we may write

$$|\varphi_{P_s}|^2=|\varphi_{P_s}{}^A|^2 F(P_s{}^2/\alpha^2+1)\,, \tag{6}$$

where $F(P_s{}^2/\alpha^2+1)$ is a power series in $(P_s{}^2/\alpha^2+1)$, and $F(0)=1$.[11]

It has been observed by Chew and Low that corrections to the deuteron cross section for reaction (3), based on final-state interactions of the spectator proton with the other outgoing particles, will have a dominant functional dependence that can be represented by a power series in $(P_s{}^2/\alpha^2+1)$, $G(P_s{}^2/\alpha^2+1)$, where $G(0)=1$.[11] However, this representation is rigorously correct only if the measurement of the cross section includes simultaneous observations of all possible spectator production angles.[11,17] Because the cross section $d^3\sigma/d\Omega_p d\Omega_\pi dP_\pi$ is determined from events in which the laboratory angle of the spectator particle relative to the directions of the other particles remains fixed, corrections to the cross sections $d^3\sigma/d\Omega_p d\Omega_\pi dP_\pi$ arising from final-state interactions may not be of the form $G(P_s{}^2/\alpha^2+1)$. However, correction terms for the cross section that are a function of odd powers of $|\mathbf{P}_s|$, if they exist, will be multiplied by angular integrals that vanish when integrated over all spectator production angles. Our final method of data analysis integrates the cross section $d^3\sigma/d\Omega_p d\Omega_\pi dP_\pi$ over our complete detector acceptance. This integration extends over a large region of spectator angles, effectively minimizing the importance of terms in the cross section which are functions of odd powers of $|\mathbf{P}_s|$. We shall assume that the final-state interactions of the spectator particle can be represented by a power series in $(P_s{}^2/\alpha^2+1)$, $G(P_s{}^2/\alpha^2+1)$. To a certain extent, we can check the validity of this approximation and the validity of other approximations which have been made in this derivation by observing whether or not our data are consistent with the form of the cross section predicted using these approximations.

Therefore, the π^- production cross section from deuterium in the laboratory system can be expressed in terms of the production cross section from a free nucleon as

$$\begin{aligned} d^3\sigma/d\Omega_p d\Omega_\pi dP_\pi &= \frac{1}{\pi^2\alpha^3}\frac{P_p{}^3 m_p}{P_\pi E_\pi}\frac{1}{(P_s{}^2/\alpha^2+1)^2}\frac{1}{(1-\alpha r_0)} \\ &\times\frac{[(E_\gamma+m_n)P_\pi{}^2-E_\pi(\mathbf{P}_\gamma\cdot\mathbf{P}_\pi)]}{[P_p{}^2(E_\gamma+m_D-E_\pi)-E_p\mathbf{P}_p\cdot(\mathbf{P}_\gamma-\mathbf{P}_\pi)]} \\ &\times\frac{d\sigma}{d\Omega_\pi}\Big|_{\text{free}} H(P_s{}^2/\alpha^2+1)\,, \end{aligned} \tag{7}$$

where

$$\begin{aligned} H(P_s{}^2/\alpha^2+1) &= F(P_s{}^2/\alpha^2+1)G(P_s{}^2/\alpha^2+1) \\ &= 1+\sum_{N=1}^{\infty} C_N(P_s{}^2/\alpha^2+1)^N. \end{aligned}$$

This formulation takes into account our limited knowledge of the deuteron wave function and the effects of final-state interactions on the cross section for the production of a π^- meson from deuterium. The coefficients C_N must be evaluated from the experimental data. However, for data in the region of small $P_s{}^2$, only the first few terms of $H(P_s{}^2/\alpha^2+1)$ should be important. Thus, this formulation allows us to determine values of the cross section for the photoproduction of π^- mesons from a free neutron from measurements of $d^3\sigma/d\Omega_p d\Omega_\pi dP_\pi$ from deuterium.

III. EXPERIMENTAL METHOD

A. General Description

For this experiment we used the bremsstrahlung beam produced by the MIT 350-MeV electron synchrotron as a source of gamma rays. In a bremsstrahlung beam, the direction of the bombarding gamma ray is fixed, but there is a spectrum of incident gamma-ray energies. Therefore, in order to completely determine the kinematics associated with the reaction

$$\gamma+D\rightarrow p+p_s+\pi^-, \tag{8}$$

[16] A. Kuckes, R. Wilson, and P. Cooper, Ann. Phys. (N. Y.) **15**, 193 (1961).
[17] F. E. Low (private communication).

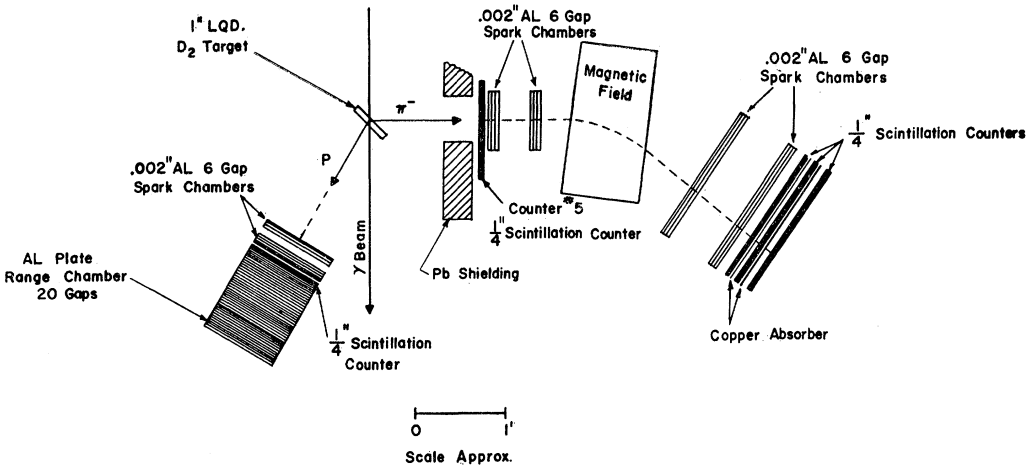

FIG. 1. Detector arrangement for $\theta_{\pi\text{lab}}\sim 96°$, $\theta_{p\text{lab}}\sim 32°$.

we had to measure six kinematic variables in addition to the known incident gamma-ray direction. This consideration, as well as those that follow, influenced our choice of particle detectors in this experiment.

If final state interactions do not play a dominant role in the production process, then the number of events, as a function of spectator momenta, will be roughly proportional to

$$N(P_s^2)\sim 1/(P_s^2/\alpha^2+1)^2. \tag{9}$$

Since the particle yields are greatest for small spectator momenta, and since the data must be categorized in terms of spectator momenta and extrapolated to $P_s^2=-\alpha^2$, we decided to accumulate events with P_s^2 between zero and five α^2. The corresponding spectator proton kinetic energies lay between 0 and 5 MeV. Because the spectator proton did not have sufficient energy to leave the deuterium target, its angle and energy could not be measured. Therefore, the six kinematic variables we measured were the momenta and angles of the π^- and those of the high-energy proton.

An investigation of the kinematics of reaction (8) showed that angular accuracies of $\pm 1°$ and large solid angles were necessary to acquire enough data points to form an extrapolation curve. Thus, the need for detectors which subtended large solid angles and also measured angles accurately led us to use spark chambers to determine particle angles.

We also used spark chambers to measure proton energy and pion momentum. Stopping protons in a range chamber enabled us to determine their energies. Pion momenta were calculated from measurements of the angles of the pions before they entered and after they left a magnetic field.

The detector arrangement for performing these measurements is diagrammed in Fig. 1. This figure shows the experimental setup with the proton detectors centered about 32° with respect to the gamma-ray beam. We also were able to center our proton detectors at angles of about 22° and 40° with respect to the gamma-ray beam. The corresponding laboratory angles of the pion detectors were 96°, 118°, and 76°, respectively. The thicknesses of the range chamber plates and the values of the magnetic field were chosen to make the central gamma-ray energy corresponding to the observed events about 275 MeV. Counter No. 5 was in place only during runs in which the chambers were triggered by single mesons traversing the magnet.

B. Beam Layout

From its source, the bremsstrahlung beam passed sequentially through a thin quartz window in the wall of the synchrotron vacuum chamber, a primary 12-in. lead collimator $\frac{3}{16}$ in. in diameter, a small sweeping magnet, a secondary collimator in the shielding wall, a thin-walled ionization chamber, another sweeping magnet, and finally through the liquid target. At the target, the beam diameter measured 1 in. and the angular divergence was $\pm\frac{1}{6}°$.

The thin-walled ionization chamber, which was automatically recharged, monitored the total beam intensity.[18] The thin-walled chamber and its integrating circuitry were calibrated against a thick-walled shower chamber which had been intercalibrated previously with monitors at the University of Illinois betatron and at the Cornell University 300-MeV electron synchrotron. This integrating system was checked against the thick chamber periodically throughout the experiment and was stable to within $\pm 2\%$. The absolute energy of the electron beam striking the bremsstrahlung target was known to within $\pm 2\%$.

C. Liquid-Deuterium Target

The type of liquid-deuterium target used in this experiment was first developed by Janes, Hyman, and

[18] H. C. Ratz, SM thesis, MIT, 1952 (unpublished).

Strumski at the MIT Synchrotron Laboratory.[19] We determined the effective thickness of the target from measurements of the particle yields from a full hydrogen cell, from the empty cell, and from polyethylene and carbon targets of known thicknesses. This method was used to compensate for any change in cell volume or cell position relative to the gamma-ray beam because of the low temperature in the area of the cell. This method measured the effective target thickness with an accuracy of $\pm 5\%$ under target conditions identical to those which existed at the time of the experiment.

D. Setting the Counter Biases

When discrimination levels were determined, the pion detectors were centered about 96° in the laboratory system, and the proton detector was centered about 32°. Discriminator calibrations were not performed when the counters were repositioned for the other two experimental setups. Nevertheless, the discriminators on the pion counters were set low enough originally to ensure 100% pion counting efficiency for all three experimental setups. The discriminator on the proton counter was also set low enough originally to ensure nearly 100% proton counting efficiency at detector angles of 32° and 40°. However, we were not sure that this setting would be low enough to maintain 100% efficiency at the 22° angle.

In order to measure the proton detector efficiency at 22° and to check our original proton-discriminator calibration, we photographed spark chamber tracks triggered only by π^- mesons. The pictures recorded whether or not the proton discriminator fired during these events. Hand scanning the pictures, we counted the number of times the proton discriminator fired when a proton track appeared in the range chamber and the number of times the discriminator failed to fire when a proton track appeared in the range chamber. This information enabled us to calculate proton counter efficiencies which were $89.8\pm 1.9\%$ at 22°, $98.4\pm 0.9\%$ at 32°, and $99.5 \pm 0.5\%$ at 40°.

E. Background Problems

The main background problem in the experiment was that of background tracks which appeared in the proton chambers from Compton electrons and electrons from Compton gamma-ray conversions. For the proton detector set at 22°, 32°, and 40°, 1.0 g/cm², 0.5 g/cm², and 0.0 g/cm,² respectively, of carbon placed in front of the proton chambers reduced the number of background tracks to a tolerable level without seriously affecting the accuracy of our proton angle measurement. In addition, the clearing voltages of the proton chambers were adjusted in order to increase the gap efficiency of the triggering proton to its highest level.

[19] G. S. Janes, L. G. Hyman, and C. J. Strumski, Rev. Sci. Instr. **27**, 527 (1956).

The background in the pion chambers was slight. In these chambers it was possible to obtain nearly 100% gap efficiency by lowering the clearing voltages, without appreciably increasing the number of background tracks.

Accidental coincidences between the proton counter and the pion counters were another source of background. To monitor the number of such coincidences, the proton counter pulse was delayed by 50 nsec with respect to the coincidence time of $\pi^- - p$ production, and the resulting coincidence rate was measured. These accidental coincidences, as well as those from the circuit monitoring $\pi^- - p$ coincidences, triggered the spark chambers. The sensitive time of the chambers was long enough to ensure equal gap efficiencies for particles which produced accidental coincidences and for those which produced apparent $\pi^- - p$ coincidences. Because the singles rates in the pion scintillators were relatively low, other types of random coincidences could be ignored when studying $\pi^- - p$ coincidences. The accidental $\pi^- - p$ coincidence rate was approximately 5% of the total number of $\pi^- - p$ counts. For runs in which the chambers were triggered by π mesons only, the dominant-chance coincident rate occurred between the counter in front of the magnet and the set of counters behind the magnet. This accidental rate was approximately 10% of the total single-meson rate.

F. Experimental Conditions During Data Runs

Experimental conditions were varied during data runs. Table I indicates the target conditions, magnet polarity settings, and scintillation-counter coincidence requirements for triggering the spark chambers during each type of run.

Data were taken under each set of conditions with each of the three different detector arrangements. Experimental arrangements and general data-taking procedures under the several sets of conditions did not vary significantly.

During the experimental runs, the beam intensity was maintained at a low level to ensure that the number of events with unrecognizable track patterns was less than a few percent of the total number of events. Most of our

TABLE I. Experimental conditions during data runs.

Contents of target	Magnet polarity	Coincidence required to trigger chambers
D_2, empty	π^-	proton+three pion counters behind magnet, counter in front of magnet not in place
H_2, empty	π^+	three pion counters behind magnet +pion counter in front of magnet
D_2, empty	π^-	three pion counters behind magnet +pion counter in front of magnet
D_2, empty	π^+	three pion counters behind magnet +pion counter in front of magnet

data were taken at an instantaneous beam intensity of about 1.3×10^9 equivalent quanta per second. At this beam intensity, we observed three π^-p coincidences per minute from the 0.5 g/cm² liquid-deuterium target. Approximately one-third of these π^-p events passed through the final fiducial volumes. A total of 15 000 π^-p triggered events was finally scanned by the computer, of which 2000 events contributed to the final P_s^2 distributions.

IV. DATA ANALYSIS

A. Picture Scanning

The spark-chamber pictures taken during our experiment were analyzed with both computer-scanning and hand-scanning techniques. The hand scanning was performed primarily to determine the computer-scanning efficiency. Otherwise, all picture scanning was done on the PDP1 computer belonging to the MIT Laboratory for Nuclear Science.

The computer scanning was performed with the "spark-chamber automatic scanning system," SPASS, developed by Deutsch *et al.*, at MIT.[20,21] However, it was necessary to modify the original SPASS system because our events were photographed by three separate cameras. Rather than change the SPASS optical system and film transport mechanisms designed to analyze two films simultaneously, we developed a tape storage system which allowed us to scan the two pion films separately from the proton film. We also developed a magnetic tape system to transfer the SPASS measurements to either the 709 or the 7090 IBM computer. These IBM machines reconstructed the events and performed various calculations necessary for final data reduction.

Once the SPASS system was properly calibrated for our pictures, scanning time, including film loading time, was less than 10 seconds per event. But although each event was scanned rapidly, other problems greatly increased the total time needed to completely analyze an event. In particular, background tracks in the proton chambers prevented the SPASS system from analyzing about 40% of the events found acceptable in hand scanning a sampling of the pictures. Although the computer recorded its reasons for the rejection of each event, the causes remained somewhat ambiguous. These ambiguities and the rejection by the computer of so many events made it impossible for us to determine accurately the scanning efficiency of the SPASS system from SPASS scanning results alone. Therefore, we utilized hand scanning to determine what fraction of the pictures contained acceptable track patterns.

Our hand-scanning method consisted of classifying track patterns and recording the length of the proton track in the range chamber for each event. From these observations and the results of the computer scanning, we calculated the computer-scanning efficiency.

By comparing the proton range spectrum obtained by hand scanning to that obtained by computer scanning, we also observed that the computer biased against high-energy protons. The pictures containing a high-energy proton track were rejected by the computer more often than those containing a low-energy proton track because pictures of high-energy protons also contained the largest proportion of background tracks. The number of background tracks became greater as the proton energy increased because the high-energy protons produced a lower specific ionization in the thin proton chambers than did the low-energy protons. The tracks of densely ionizing particles have a higher gap efficiency and appear with fewer weakly ionized background tracks than tracks of weakly ionizing particles because the probability of spark formation along the path of the particle is proportional to the number of ion pairs produced by the particle in the spark chamber gas.

To account for the biases introduced into the proton range spectra by the computer, the spectra were normalized to the range spectra obtained by hand scanning. The effects of this normalization on our final results are discussed in Sec. IVD. The ratios of the computer-scanned range spectra to the hand-scanned range spectra for each of the three experimental setups appear in Fig. 2.

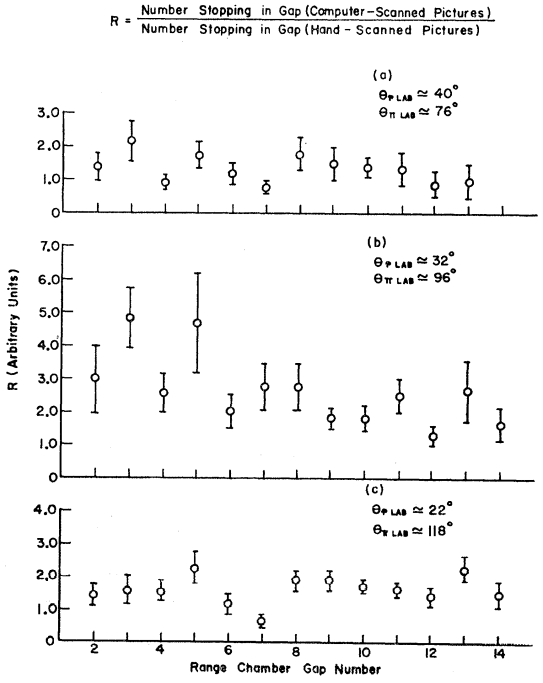

FIG. 2. Ratios of computer-scanned proton range spectra to hand-scanned range spectra.

[20] M. Deutsch, *Proceedings of the Conference on Photon Interactions in the BeV-Energy Range* (Laboratory for Nuclear Science, Massachusetts Institute of Technology, Cambridge, Massachusetts, January 1963), p. VII. 18.

[21] H. Rudloe, M. Deutsch, and T. Marrill, Comm. Assoc. Computing Machinery **6**, 332 (1963).

B. Event Rejection

In scanning our pictures, the computer could not differentiate among the pictures of events triggered by μ mesons and particles originating outside the deuterium target and the pictures of events triggered by pions and protons germane to our experiment. Therefore, it was necessary for us to make such a differentiation in our data.

To eliminate from the data as many μ-meson events as possible and to estimate the number of remaining muon events and their effects on our data, we made several track extrapolations and magnet consistency checks.

Our first consistency check was based on the following fact: In a uniform magnetic field, the components of the momentum of a particle parallel to and in a plane perpendicular to the magnetic field remain constant. In contrast, a muon from a pion decay in the magnet does not necessarily have the same component ratio as does its parent. Thus, by comparing the component ratios calculated from measurements of tracks appearing in the chambers in front of and behind the magnet, we eliminated some of the μ mesons produced by parent pions decaying between the two sets of pion chambers.

Our second consistency check depended on the following observations: The displacement Δx of the pion trajectory as a pion crosses the magnetic field can be predicted from the track angles measured in the pion chambers in front of and behind the magnetic field and the line integral of the magnetic field; and Δx can be determined by extrapolating the tracks appearing in the pion chambers (see Fig. 3).

If a pion decays between the two sets of chambers, the track displacements calculated by these two methods may differ. For a consistency check, we compared these displacements calculated for each event, and thus separated out additional μ-meson events.

Last, other μ-meson events were eliminated by requring that the pion track extrapolate back to the deuterium target.

There was approximately a 17% muon contamination in our data before events were rejected according to these criteria. After imposing rejection criteria on our events, the final muon contamination in our data was about 5%.

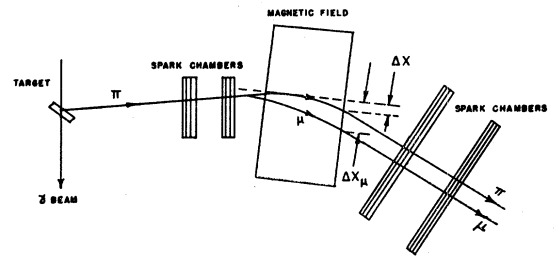

FIG. 3. Definition of Δx.

TABLE II. Uncertainties in kinematic variables considered in resolution calculations.

Kinematic variables	Causes of measurement inaccuracies taken into account
θ_p, φ_p, θ_π, φ_π	(a) multiple scattering in target (b) computer track coordinate measurements
P_π	(a) computer track coordinate measurements (b) multiple scattering in pion chambers (c) instability and nonuniformities in magnetic field (d) uncertainty in pion energy losses in target
P_p	(a) thickness of range chamber plates (b) uncertainty in proton energy losses in target (c) proton multiple scattering

The proton tracks were also extrapolated to check whether or not they originated in the deuterium target. The number of proton tracks that did not appear to originate in the target was less than 1% of the total number of events.

C. P_s^2 Resolution

For each of the three experimental setups, the resolution in the square of the momentum of the spectator P_s^2 of our detector system was calculated as a function of P_s^2. Table II shows the inaccuracies in our measurements of laboratory kinematic variables which were taken into account in these calculations.

In our calculations, we assumed that our measurement errors obeyed Gaussian distributions. Thus, we calculated the errors in our P_s^2 measurement $r(P_s^2)$ using the formula

$$r(P_s^2)=\left[\sum_i\left(\frac{\partial P_s^2}{\partial x_i}\delta x_i\right)^2\right]^{1/2}, \tag{10}$$

where the x_i's are the independent parameters that determine P_s^2, and the δx_i's are the related standard deviations. For each experimental setup, the quantity $r(P_s^2)$ was calculated for each event in a sample of approximately 30 events. The quantity $r(P_s^2)$ versus P_s^2 was then plotted for each event, and a curve $\Sigma(P_s^2)$ was drawn through the points. The resolution, $\Sigma(P_s^2)$, as a function of P_s^2 obtained by this method could be represented by the same curve $\Sigma(P_s^2)$ for all three experimental setups.

From this resolution function $\Sigma(P_s^2)$ we calculated an approximate resolution matrix for our system $R(P_s^2,P_s'^2,\delta P_s^2)$, namely

$$R(P_s^2,P_s'^2,\delta P_s^2)=\int_{P_s^2|\text{lower}}^{P_s+\delta P_s/2}\frac{Y(P_s'^2,\delta P_s^2)}{\Sigma(P_s'^2)}\times\exp\left[\frac{-(P_s'^2-P_s''^2)^2}{2[\Sigma(P_s'^2)]^2}\right]dP_s''^2, \tag{11}$$

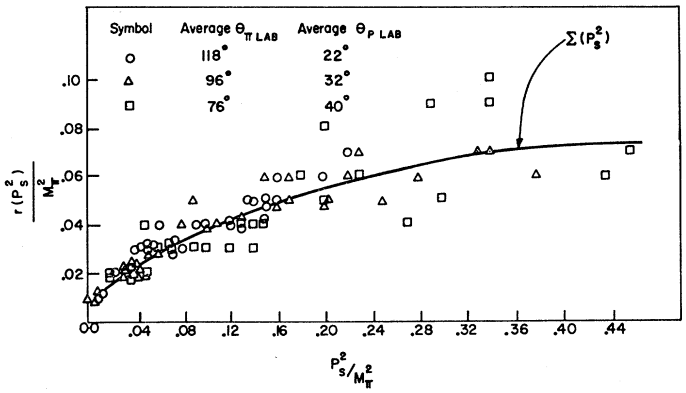

FIG. 4. P_s^2 resolution, $\Sigma(P_s^2)$, as a function of P_s^2.

where

$$P_s^2|_{\text{lower}}=P_s^2-\delta P_s^2/2 \quad \text{if} \quad P_s^2-\delta P_s^2/2\geq 0,$$
$$0 \quad \text{if} \quad P_s^2-\delta P_s^2/2<0,$$

and $Y(P_s'^2,\delta P_s^2)$ was chosen to ensure that

$$\sum_{P_s^2=0}^{\infty} R(P_s^2,P_s'^2,\delta P_s^2)=1.$$

We chose $\delta P_s^2=\frac{1}{2}\alpha^2$ to calculate the resolution matrix used in our final data reduction because our final bin widths in P_s^2 were equal to approximately α^2. The resolution function $\Sigma(P_s^2)$ and the points from which it was derived are shown in Fig. 4.

D. π^--p Data Reduction Method and Extrapolation Curves

In Sec. II, we derived an expression relating the cross section for π^- photoproduction from deuterium to the cross section for π^- photoproduction from a free neutron. This expression is

$$\frac{d^3\sigma}{d\Omega_p d\Omega_\pi dP_\pi}=\frac{d\sigma(w,\theta_{\text{c.m.}})}{d\Omega_\pi}\bigg|_{\text{free}}\frac{1}{(P_s^2/\alpha^2+1)^2}$$
$$\times f(P_p,\theta_p,\varphi_p,P_\pi,\theta_\pi,\varphi_\pi)H(P_s^2/\alpha^2+1), \quad (12)$$

where

$$f(P_p,\theta_p,\varphi_p,P_\pi,\theta_\pi,\varphi_\pi)=\frac{1}{\alpha^3\pi^2(1-\alpha r_0)}\frac{P_p{}^3m_p}{P_\pi E_\pi}$$
$$\times\frac{[(E_\gamma+m_n)P_\pi{}^2-E_\pi(\mathbf{P}_\gamma\cdot\mathbf{P}_\pi)]}{[P_p{}^2(E_\gamma+m_D-E_\pi)-E_p\mathbf{P}_p\cdot(\mathbf{P}_\gamma-\mathbf{P}_\pi)]},$$

and

$$H(P_s^2/\alpha^2+1)=1+\sum_{N=1}^{\infty}C_N(P_s^2/\alpha^2+1)^N.$$

If we assume that the spectator particle plays little or no role in the production process, then we may neglect all the coefficients C_N except C_1. We will be able to check the validity of this assumption by observing whether or not our data are consistent with the predictions of Eq. (12) when it contains only the two unknown parameters, $d\sigma(w,\theta_{\text{c.m.}})/d\Omega_\pi|_{\text{free}}$ and C_1. To perform this consistency check and to determine the free cross section, we must formulate extrapolation curves from our data with the following calculations.

First, for given detector acceptances, we can relate the number of events observed with P_s^2 between $P_s^2-\delta P_s^2/2$ and $P_s^2+\delta P_s^2/2$, $N(P_i^2,\delta P_s^2)$, to the unknown cross section, $d\sigma(w,\theta_{\text{c.m.}})/d\Omega_\pi|_{\text{free}}$, and the parameter C_1 by the expression

$$N(P_s^2,\delta P_s^2)=\int_{R,P_s^2,\delta P_s^2}\frac{d\sigma(w',\theta_{\text{c.m.}}')}{d\Omega_\pi}\bigg|_{\text{free}}$$
$$\times\frac{1}{(P_s'^2/\alpha^2+1)^2}[1+C_1(P_s'^2/\alpha^2+1)]$$
$$\times f(P_p',\theta_p',\varphi_p',P_\pi',\theta_\pi',\varphi_\pi')(\partial E_\gamma'/\partial P_p')$$
$$\times(\phi(E_\gamma')/E_\gamma')Q_0t_0d\Omega_p'dP_p'd\Omega_\pi'dP_\pi', \quad (13)$$

where

$$[Q_0\phi(E_\gamma')/E_\gamma'](\partial E_\gamma'/\partial P_p')dP_p'$$

is the number of incident gamma rays with energies between E_γ' and $E_\gamma'+dE_\gamma'$, t_0 is the number of deuterium nuclei per square centimeter in the target, and Q_0 is the total number of equivalent quanta that passed through the target. The bremsstrahlung function $\phi(E_\gamma')$ is that calculated by Tabakin[22] from the cross section calculated by Olsen, Maximon, and Wergeland,[23] taking into account the thick target corrections of Wilson.[24] The integral in expression (13) is carried out over the complete detector system energy and angle acceptance, R, in such a way that

$$P_s^2-\delta P_s^2/2\leq P_s'^2\leq P_s^2+\delta P_s^2/2 \quad \text{if} \quad P_s^2-\delta P_s^2/2\geq 0,$$

and

$$0\leq P_s'^2\leq P_s^2+\delta P_s^2/2 \quad \text{if} \quad P_s^2-\delta P_s^2/2<0.$$

[22] F. Tabakin (private communication).
[23] H. Olsen, L. C. Maximon, and H. Wergeland, Phys. Rev. **106**, 27 (1957).
[24] R. Wilson, Proc. Roy. Soc. (London) **A66**, 638 (1953).

Also, if we assume that $d\sigma(w',\theta_{\text{c.m.}}')/d\Omega_\pi|_{\text{free}}$ remains constant over the region of integration, then we can write

$$N(P_s^2,\delta P_s^2)=\left.\frac{d\sigma(w,\theta_{\text{c.m.}})}{d\Omega_\pi}\right|_{\text{free}} \times[A(P_s^2,\delta P_s^2)+C_1B(P_s^2,\delta P_s^2)], \quad (14)$$

where

$$A(P_s^2,\delta P_s^2)=\int_{R,P_s^2,\delta P_s^2}\frac{f(P_p',\theta_p',\varphi_p',P_\pi',\theta_\pi',\varphi_\pi')}{(P_s'^2/\alpha^2+1)^2} \times\frac{\partial E_\gamma'}{\partial P_\gamma'}\frac{\phi(E_\gamma')}{E_\gamma'}t_0Q_0d\Omega_p'dP_p'd\Omega_\pi'dP_\pi',$$

and

$$B(P_s^2,\delta P_s^2)=\int_{R,P_s^2,\delta P_s^2}\frac{f(P_p',\theta_p',\varphi_p',P_\pi',\theta_\pi',\varphi_\pi')}{(P_s'^2/\alpha^2+1)} \times\frac{\partial E_\gamma'}{\partial P_p'}\frac{\phi(E_\gamma')}{E_\gamma'}t_0Q_0d\Omega_p'dP_p'd\Omega_\pi'dP_\pi'.$$

In performing the integrations necessary to calculate $A(P_s^2,\delta P_s^2)$ and $B(P_s^2,\delta P_s^2)$, we tabulate the interval over which w' and $\theta_{\text{c.m.}}'$ vary. A knowledge of these intervals allows us to assign to the free cross section $d\sigma(w,\theta_{\text{c.m.}})/d\Omega_\pi$, an average production angle and an average bombarding gamma-ray energy.

Because $A(P_s^2,\delta P_s^2)$ is a rapidly varying function of P_s^2, we can not compare directly the measured P_s^2 distribution of our events to $N(P_s^2,\delta P_s^2)$. We therefore consider the effect of the P_s^2 resolution of our detector system on the observed P_s^2 distribution $N_{\text{obs}}(P_s^2,\delta P_s^2)$. The spectrum $N_{\text{obs}}(P_s^2,\delta P_s^2)$ is related to the true spectrum $N(P_s^2,\delta P_s^2)$ by the relationship

$$N_{\text{obs}}(P_s^2,\delta P_s^2)=\sum_{P_s'^2=0}^{\infty}R(P_s^2,P_s'^2,\delta P_s^2)N(P_s'^2,\delta P_s^2), \quad (15)$$

where $R(P_s^2,P_s'^2,\delta P_s^2)$ is the resolution matrix as defined in Sec. IVC.

Thus,

$$N_{\text{obs}}(P_s^2,\delta P_s^2)=\left.\frac{d\sigma(w,\theta_{\text{c.m.}})}{d\Omega_\pi}\right|_{\text{free}}\left[\sum_{P_s'^2}R(P_s^2,P_s'^2,\delta P_s^2) \times\{A(P_s'^2,\delta P_s^2)+C_1B(P_s'^2,\delta P_s^2)\}\right], \quad (16)$$

or

$$N_{\text{obs}}(P_s^2,\delta P_s^2)=\left.\frac{d\sigma(w,\theta_{\text{c.m.}})}{d\Omega_\pi}\right|_{\text{free}} \times[a(P_s^2,\delta P_s^2)+C_1b(P_s^2,\delta P_s^2)], \quad (17)$$

where

$$a(P_s^2,\delta P_s^2)=\sum_{P_s'^2}R(P_s^2,P_s'^2,\delta P_s^2)A(P_s'^2,\delta P_s^2)$$

and

$$b(P_s^2,\delta P_s^2)=\sum_{P_s'^2}R(P_s^2,P_s'^2,\delta P_s^2)B(P_s'^2,\delta P_s^2).$$

The importance of the P_s^2 resolution in the final data reduction can be seen from Fig. 5. In the limit of infinitely accurate P_s^2 measurements, the ratio $a(P_s^2,\delta P_s^2)/A(P_s^2,\delta P_s^2)$ becomes equal to 1, and $b(P_s^2,\delta P_s^2)/a(P_s^2,\delta P_s^2)$ approaches (P_s^2/α^2+1). We can see from Fig. 5 that resolution effects do not influence our results a great deal. Because resolution effects are not important, it is true that within approximately 2%,

$$b(P_s^2/\alpha^2+1)/a(P_s^2/\alpha^2+1)\simeq(P_s^2/\alpha^2+1). \quad (18)$$

Therefore, if we perform a linear fit to the data points, $N_{\text{obs}}(P_s^2,\delta P_s^2)/a(P_s^2,\delta P_s^2)$, the value of this curve at the point $P_s^2=-\alpha^2$ will be $d\sigma(w,\theta_{\text{c.m.}})/d\Omega_\pi|_{\text{free}}$.

Before the extrapolation curves were plotted, observed events were corrected for μ-meson contamination, pion and proton losses due to nuclear absorption, pion losses from pion decay in flight, computer scanning efficiency, and computer proton range spectrum biases. The corrections to the experimentally observed P_s^2 distributions resulting from the normalization of the computer-scanned range spectra are shown in Fig. 6. The fluctuations in these corrections are a rough indication of the uncertainty, introduced into the corrected P_s^2 distribution, arising from the statistical uncertainties in the proton range spectrum. Because these fluctuations are small compared to the statistical accuracy of the P_s^2 distributions, we neglect any error introduced into the P_s^2 distributions by our normalization of the computer-scanned range spectra.

The extrapolation curves formed in this way are shown in Fig. 7. Both linear and constant fits, $C_1=0$, to the data have been performed. The results for the "free" neutron cross sections are listed in Table III, where χ^2/F is the chi squared of the fit divided by the number of degrees of freedom. From the values of χ^2/F,

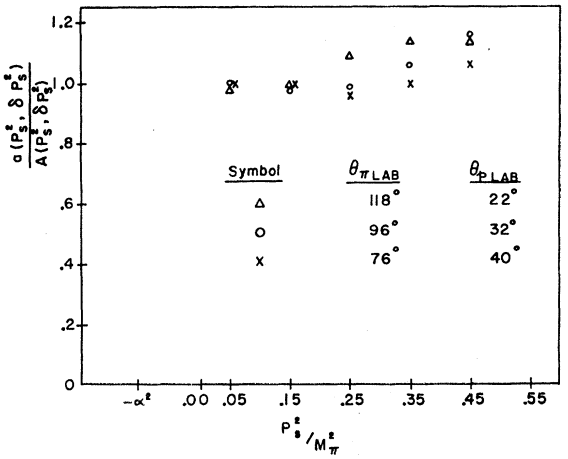

FIG. 5. $a(P_s^2,\delta P_s^2)/A(P_s^2,\delta P_s^2)$ as a function of P_s^2.

TABLE III. Extrapolated laboratory cross sections for the reaction $\gamma+n \rightarrow \pi^-+p$. $\theta_{\pi c.m.}$ is the angle between the incident gamma ray and the pion in the $\gamma-n$ center-of-mass system. χ^2/F is the chi-squared of the fit divided by the number of degrees of freedom.

Type of fit	$\theta_{\pi\ c.m.}$	Bombarding gamma-ray energies (MeV)	Extrapolated value of $d\sigma/d\Omega_{\pi lab}$ (μb/sr)	Error in $d\sigma/d\Omega_{\pi lab}$ resulting from uncertainties in the value of the extrapolation curve at $P_s^2=-\alpha^2$ (μb/sr)	Estimated total error in $d\sigma/d\Omega_{\pi lab}$ (μb/sr)	χ^2/F
Constant ($C_1=0$)	92°	275±22	18.8	±0.9	±2.8	1.6
Constant	112°	275±21	16.4	±0.7	±2.5	1.5
Constant	132°	275±18	12.2	±0.5	±1.8	0.8
Linear	92°	275±22	15.1	±2.3	±3.1	1.1
Linear	112°	275±21	16.0	±1.7	±2.9	2.0
Linear	132°	275±18	11.7	±1.6	±2.5	1.1

we can see that our data are consistent with constant fits. However, at $\theta_{\pi c.m.}=92°$, the linear fit is slightly better. The total error in $d\sigma/d\Omega_\pi|_{\text{free}}$ listed in Table III includes, in addition to the extrapolation error, uncertainties which affect only the normalization of the extrapolation curve. The uncertainties that give rise to the total error in the cross sections are listed in Table IV.

For the remainder of this paper, we consider the cross sections given by constant fits to be representative of our data. Because the cross sections derived from constant fits and the cross sections derived from linear fits agree within assigned errors, this choice is inconsequential when our results for the "free" cross sections are compared to the predictions of dispersion theory.

In evaluating the results of the extrapolation procedure, the following facts should be considered. First, if the true deuteron wave function is approximated by a Hulthén wave function instead of the pole term alone, the pole term, $1/(P_s^2/\alpha^2+1)^2$, of Eq. (12) is replaced by

$$\frac{1}{(P_s^2/\alpha^2+1)^2}\left[1-\frac{2\alpha^2}{\beta^2}(P_s^2/\alpha^2+1)\right],$$

where α^2/β^2 is equal to 0.045. This type of analysis would require linear fits to our data but would yield "free" cross sections in agreement with those obtained using only the pole term. Because a choice between the two methods is somewhat arbitrary, it is difficult to determine the significance of the fact that the pole approximation fits our data without any linear correction terms.[16]

Second, for backward pion production angles, the "free" negative to positive ratio obtained from this experiment, see Fig. 8, is not equal to the ratio of the cross sections,

$$\frac{d^2\sigma(\gamma+D\rightarrow 2p+\pi^-)}{d\Omega_\pi dP_\pi}\Big/\frac{d^2\sigma(\gamma+D\rightarrow 2n+\pi^+)}{d\Omega_\pi dP_\pi},$$

measured using bremsstrahlung, see Table V. However, our results for the "free" ratios agree with the results obtained by Land using monochromatic gamma rays.[7] This agreement and the fact that both experiments disagree with the measured bremsstrahlung ratios,

$$\frac{d^2\sigma(\gamma+D\rightarrow 2p+\pi^-)}{d\Omega_\pi dP_\pi}\Big/\frac{d^2\sigma(\gamma+D\rightarrow 2n+\pi^+)}{d\Omega_\pi dP_\pi},$$

indicates the necessity of performing an extrapolation

TABLE IV. Origin of total errors assigned to extrapolated cross sections.

Origin of uncertainty	% error
(a) Extrapolation error	± 5.0
(b) Proton angle and energy acceptance	± 5.0
(c) Picture-scanning efficiency	±10.0
(d) Proton scintillator efficiency	± 2.0
(e) Proton nuclear absorption losses	± 2.0
(f) Pion angle and energy acceptance	± 5.0
(g) Pion decay in flight correction	± 2.0
(h) Pion scintillation efficiencies	± 2.0
(i) Pion nuclear absorption losses	± 1.0
(j) Beam monitoring	± 3.0
(k) Target thickness	± 5.0
(l) μ-meson contamination	± 5.0

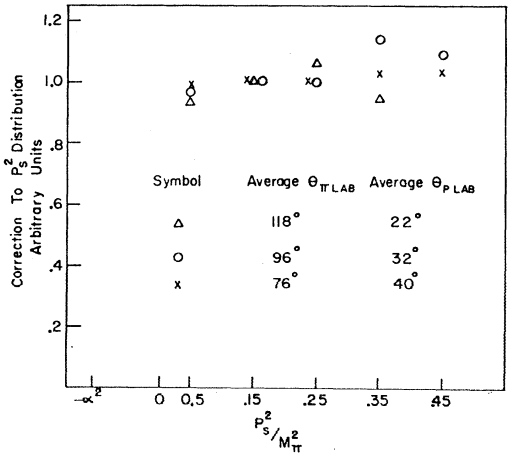

FIG. 6. Corrections for experimental P_s^2 distributions resulting from range spectra normalizations.

experiment, or at least an experiment of the type performed by Land, in determining the "free" neutron cross sections in this energy region.

E. Additional Data

In addition to measuring the $\pi^- - p$ photoproduction cross sections from deuterium, we performed measurements of single pion production cross sections from hydrogen and deuterium. In particular, we measured the absolute cross section for π^+ photoproduction from hydrogen and the cross sections, $d^2\sigma/d\Omega_\pi dP_\pi$, for π^+ and π^- production from deuterium relative to the cross section $d^2\sigma/d\Omega_{\pi^+}dP_{\pi^+}$ from hydrogen.

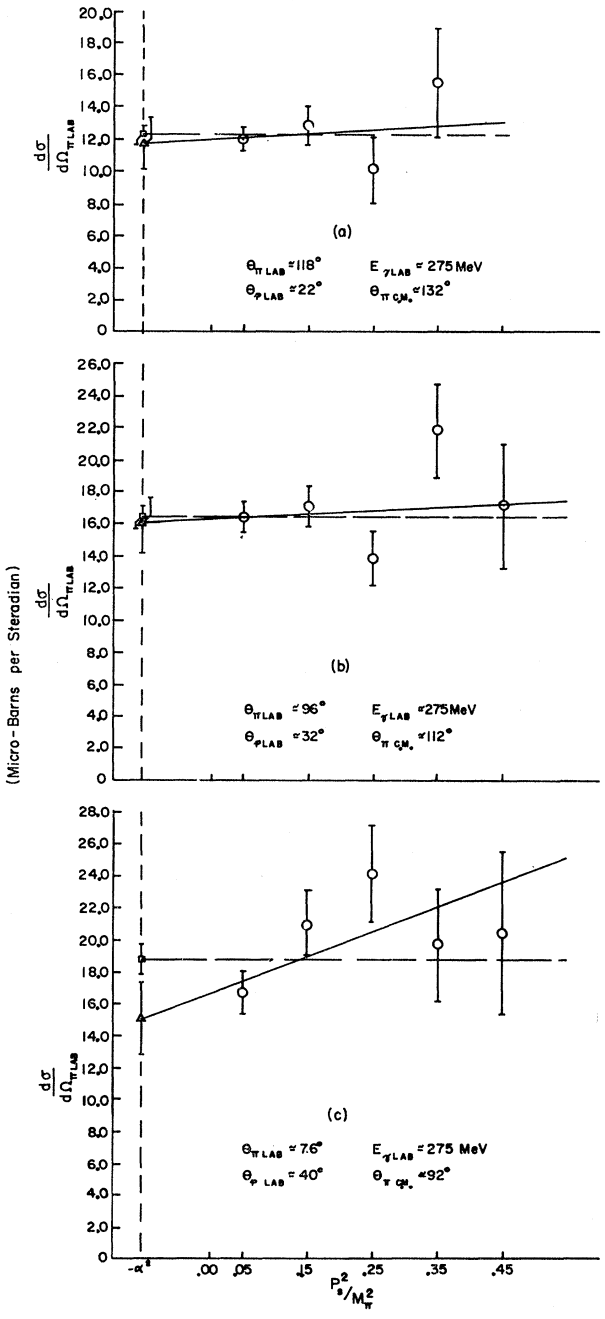

FIG. 7. Extrapolation curves for determining free neutron cross sections. The extrapolated cross sections for constant and linear fits are the points plotted at $P_s^2=-\alpha^2$. Uncertainties affecting only the over-all normalization of the extrapolation curve were not included in the calculation of the error bars.

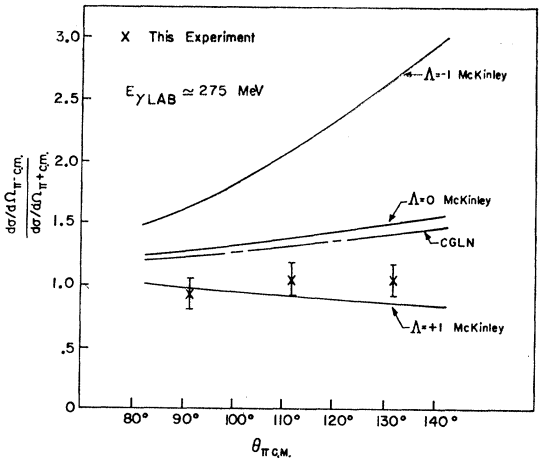

FIG. 8. Results for the negative to positive ratio for free nucleons. The numerical values of the CGLN theory were calculated by L. Hand, Ref. 34. The numerical values of McKinley's theory were calculated by F. F. Liu using McKinley's Y set of phase shifts (Ref. 33).

The apparatus used in these measurements was the same as that used in the $\pi^- - p$ measurements. However, for determining the single-particle cross sections it was only necessary to use the pion spectrometer.

The relative cross sections, $d^2\sigma/d\Omega_\pi dP_\pi$, were determined from the observed counting rates of full and empty target runs. The relative cross sections determined in this way using 318-MeV bremsstrahlung are shown in Table V.

The absolute hydrogen cross sections were obtained from the hydrogen events by the following method. First, events photographed with the target full and events photographed with the target empty were hand scanned to determine the fraction of coincident pions that passed through the fiducial volumes of the spark chambers. Second, the μ-meson contamination of these events was estimated from the known μ-meson contamination of the measured $\pi^- - p$ events. Third, the events were corrected for pion decay in flight and nuclear absorption losses. Finally, other experimental determinations of the π^+ photoproduction cross sections in the angle and energy regions of our experiment were consistent with a cross section energy dependence of the form

$$\frac{d\sigma(E_{\gamma\text{lab}},\theta_{\pi\text{lab}})}{d\Omega_{\pi\text{lab}}}=\frac{d\sigma(E_0,\theta_{\pi\text{lab}})}{d\Omega_{\pi\text{lab}}}[1+a_0(E_{\gamma\text{lab}}-E_0)], \quad (19)$$

where $E_0=275$ MeV. This allowed us to calculate the cross sections for π^+ photoproduction by 275-MeV

TABLE V. Relative photomeson cross sections measured using 318 MeV bremsstrahlung.

$\theta_{\pi\text{lab}}$	$P_{\pi\text{lab}}$(MeV/c)	ΔP_π(MeV/c)	$\frac{d^2\sigma(\gamma+D\to 2n+\pi^+)}{d\Omega_\pi dP_\pi} \Big/ \frac{d^2\sigma(\gamma+p\to\pi^++n)}{d\Omega_\pi dP_\pi}$	$\frac{d^2\sigma(\gamma+D\to 2p+\pi^-)}{d\Omega_\pi dP_\pi} \Big/ \frac{d^2\sigma(\gamma+D\to 2n+\pi^+)}{d\Omega_\pi dP_\pi}$
118°	160	±23	0.63±0.05	1.46±0.10
96°	168	±27	0.83±0.09	1.23±0.08
76°	188	±29	0.78±0.06	0.97±0.08

gamma rays from the following relationship:

$$\text{Number of events}=\frac{d\sigma(E_0,\theta_{\pi\text{lab}})}{d\Omega_{\pi\text{lab}}}A\,,$$

where

$$A=\int_R[1+a_0(E_{\gamma\text{lab}}-E_0)]t_0Q_0 \times\frac{\phi(E_{\gamma\text{lab}})}{E_{\gamma\text{lab}}}\frac{\partial E_{\gamma\text{lab}}}{\partial P_{\pi\text{lab}}}d\Omega_{\pi\text{lab}}dP_{\pi\text{lab}}. \quad (20)$$

The integration was performed over the entire pion acceptance R and the quantities appearing in the integral are defined in Sec. IVD.

The cross sections found by this method are listed in Table VI. The uncertainty in their values resulting from statistical counting errors is approximately ±5%. The uncertainty arising from our use of the empirical energy dependence, expression (19), is less than 3%.

Finally, the hydrogen cross sections, as well as the relative cross sections for π^+ and π^- production, are in good agreement with other determinations of these cross sections.[1–9,25]

V. COMPARISON OF EXPERIMENTAL RESULTS WITH DISPERSION THEORY

At present, the most reliable theoretical predictions[12] of cross sections for photoproduction of single π mesons from nucleons are based on dispersion theory. The original work of Chew, Goldberger, Low, and Nambu, hereafter CGLN, explained successfully the qualitative features of π^+ and π^0 photoproduction cross sections for bombarding gamma-ray energies below 350 MeV.[26]

TABLE VI. Measured cross sections for reaction $\gamma+p\to\pi^++n$.

$E_{\gamma\text{lab}}\simeq$275 MeV		
$\theta_{\pi\text{c.m.}}$	$d\sigma/d\Omega_{\pi\text{c.m.}}$ (μb/sr)	Total error (μb/sr)
92°	18.7	±2.0
112°	17.7	±1.9
132°	16.7	±1.8

However, their theory predicted a coefficient too small for the cosine squared term in the low-energy π^0 angular distributions and values too large for the π^+ differential cross sections at backward angles for all energies.[26]

These quantitative discrepancies led to investigation of effects of the small nonresonant $\pi-N$ scattering phase shifts on the theoretical photoproduction cross sections.[27–30] By replacing the CGLN effective-range phase shifts with the experimentally determined phase shifts, better agreement between photoproduction experiment and theory was achieved.

In order to examine the validity of using experimental π-nucleon scattering phase shifts in predicting photoproduction cross sections, McKinley performed a new derivation of the photoproduction amplitudes.[26] His approach is almost identical to that of CGLN, but he does not make use of an expansion in the ratio of the meson to nucleon masses, and he introduces a comparison function in the relation between the resonant scattering and the resonant photoproduction amplitudes. This comparison function enables McKinley to relate exactly the resonant (3,3) scattering and resonant (3,3) photoproduction amplitudes. Unfortunately, these improvements in the original CGLN theory do not increase the agreement between experiment and theory.

McKinley also attempted to account for the effects of the ρ meson on the photoproduction cross sections, using a method similar to that of De Tollis and Verganelakis.[31,32] In particular, a term is added to the F_0 amplitude of CGLN which is proportional to the unknown decay rate of the ρ meson into a π meson and a gamma ray. This term contains a parameter Λ which is proportional to the $\rho\gamma\pi$ coupling constant.

For the purposes of comparison, we have plotted the results of this experiment for the "free" negative to positive ratio, together with McKinley's predicted ratios for different values of the coupling constant Λ[33]

[25] R. L. Walker, J. G. Teasdale, V. Z. Peterson, and J. I. Vette, Phys. Rev. **99**, 210 (1955).

[26] J. M. McKinley, Technical Report No. 38, Contract ONR-1834(05), Physics Department, University of Illinois, May 1962 (unpublished).

[27] A. J. Lazarus, W. K. H. Panofsky, and F. R. Tangherlini, Phys. Rev. **113**, 1330 (1959).

[28] J. L. Uretsky, R. W. Kenney, E. A. Knapp, and V. Perez-Mendz, Phys. Rev. Letters **1**, 12 (1958).

[29] C. S. Robinson, P. M. Baum, L. Criegee, and J. M. McKinley, Phys. Rev. Letters **9**, 349 (1962).

[30] R. C. Smith and R. F. Mozley, Phys. Rev. **130**, 2429 (1963).

[31] B. De Tollis and A. Verganelakis, Nuovo Cimento **22**, 406 (1961).

[32] B. De Tollis and A. Verganelakis, Phys. Rev. Letters **6**, 371 (1961).

[33] The numerical evaluation of McKinley's formulas was performed by F. F. Liu using McKinley's Y set of phase shifts (private communication).

and the predicted ratios of CGLN,[34] in Fig. 8. From this figure we can see that our results for the "free" negative-to-positive ratio disagree with the predictions of CGLN. McKinley's calculations are consistent with our measured ratios only if Λ is positive and is valued near 0.75. It should be emphasized that the theoretical values for the negative-to-positive ratios are not affected significantly by uncertainties in the pion-nucleon coupling constant, the position of the first resonance, or the values of the small pion-nucleon scattering phase shifts.[35]

Our results for the absolute cross sections for the reactions

$$\gamma+n\rightarrow\pi^-+p$$

and

$$\gamma+p\rightarrow\pi^+ +n$$

are shown in Figs. 9 and 10 along the predictions of CGLN and the predictions of McKinley. From these figures we can conclude that CGLN do not predict the charged meson cross sections correctly and that McKinley's calculations cannot fit both the π^+ and π^- cross sections with one value of Λ. Uncertainties in the

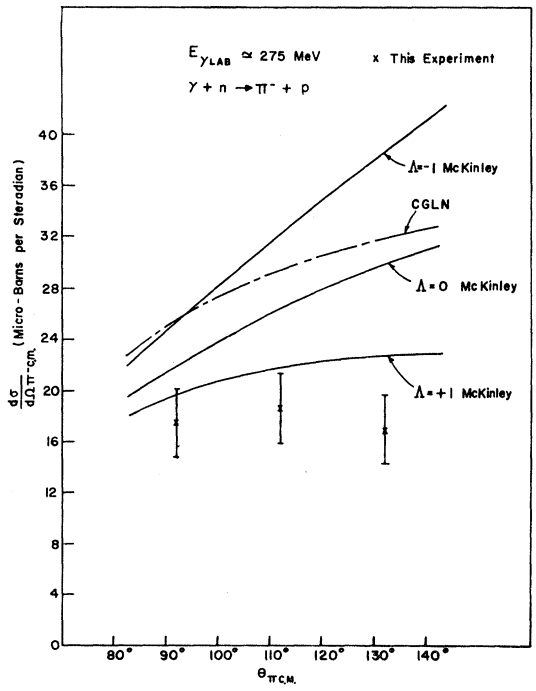

FIG. 9. Measured differential cross sections for the reaction $\gamma+n\rightarrow\pi^-+p$.

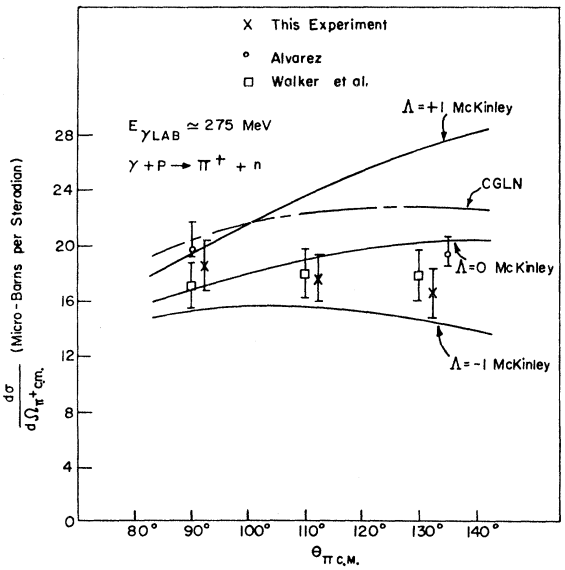

FIG. 10. Measured differential cross sections for the reaction $\gamma+p\rightarrow\pi^+ +n$. For comparison, the results of Alvarez [R. A. Alvarez, Bull. Am. Phys. Soc. 9, 70 (1964)] and Walker *et al.* (Ref. 25), are shown.

pion-nucleon coupling constant, in the position of the first resonance, and in the small phase shifts give rise to an uncertainty of approximately $\pm 15\%$ for the predicted cross sections in the angle and energy region of our data.[29] This small theoretical uncertainty does not bring the CGLN and McKinley calculations into agreement with our results. Apparently, better quantitative agreement between dispersion theory and photomeson experiments awaits a deepening in the theoretical understanding of the influence of high-energy pion-nucleon resonances, strange particles, and other resonant elementary particle states on the cross sections.

ACKNOWLEDGMENTS

We are indebted to Professor Louis S. Osborne for suggesting this problem and for his guidance and assistance throughout the experiment. The efforts of Professor Martin Deutsch and his group were invaluable in making possible computer scanning of the spark-chamber photographs. Discussions with Professor Raymond Alvarez were helpful in clarifying some of the experimental and theoretical problems of low-energy pion physics. J. Uglum, W. Lobar, C. Strumski, D. Cook, R. Renbeck, and G. Krebs helped construct and maintain the experimental apparatus; and R. McEntire, H. Rudloe, and R. Greibach wrote computer programs for data analysis. The MIT Computation Center generously provided time on their 7090 IBM computer for part of this work.

[34] The numerical evaluation of the CGLN formulas was performed by L. Hand (private communication). The phase shifts used are those described by L. Hand, Phys. Rev. **129**, 1834 (1963).

[35] J. Pine and M. Bazin, Phys. Rev. **132**, 2735 (1963).